The 9th European Congress on Computational Methods in Applied Sciences and Engineering
ECCOMAS Congress 2024
3–7 June 2024, Lisboa, Portugal

# FRACTIONAL FLOW RESERVE PREDICTION USING IN-HOUSE COMPUTATIONAL METHODS - VALIDATION WITH SEVERAL PATIENT CASES

**MARIA FERNANDES[1], LUÍSA C. SOUSA[2] AND SÓNIA I.S. PINTO[3]**

[1] Faculty of Engineering of the University of Porto (FEUP)
Rua Dr. Roberto Frias s/n, Porto, Portugal

Institute of Science and Innovation in Mechanical and Industrial Engineering (INEGI)
Rua Dr. Roberto Frias 400, Porto, Portugal e-mail: mcfernandes@fe.up.pt

[2] Faculty of Engineering of the University of Porto (FEUP)
Rua Dr. Roberto Frias s/n, Porto, Portugal

Institute of Science and Innovation in Mechanical and Industrial Engineering (INEGI)
Rua Dr. Roberto Frias 400, Porto, Portugal e-mail: lcsousa@fe.up.pt

[3] Faculty of Engineering of the University of Porto (FEUP)
Rua Dr. Roberto Frias s/n, Porto, Portugal

Institute of Science and Innovation in Mechanical and Industrial Engineering (INEGI)
Rua Dr. Roberto Frias 400, Porto, Portugal e-mail: spinto@fe.up.pt

**Key words:** Numerical Simulations, Fractional Flow Reserve, Windkessel Model, Viscoelastic Property of Blood, Coronary Arteries, Atherosclerosis

**Summary.** The Fractional Flow Reserve (FFR) serves as a critical parameter for evaluating stenosis severity. However, the invasive nature of the procedure used to obtained it poses risks to patients. Therefore, developing computational tools for FFR calculation is valuable to clinicians. The goal of this research is to validate an in-house computational tool designed to predict FFR numerically using complex models to simulate real patient-specific physiological blood flow in coronary artery 3D models, including a simplified Phan-Thien/Tanner model for viscoelastic blood properties and a three-element Windkessel model for outlet pressure. By the qualitative comparison of the computed and invasive FFR ranges, the accuracy, sensitivity, and specificity of the tool were equal to 1. These are promising results that indicate that this numerical tool could, eventually, replace the invasive procedure of measuring the FFR.

## 1 INTRODUCTION

The numerical study of blood flow in coronary arteries with atherosclerosis could aid diagnosis in an easier and cheaper way than invasive methods. Several methods have been studied and employed in the literature [3, 4, 5]. The fractional flow reserve (FFR) is a parameter used by cardiologists to determine the functional severity of stenosis in blood vessels. This parameter aids medical doctors in the diagnosis of coronary artery diseases, like atherosclerosis, through

the functional assessment of the stenosis. FFR values below 0.75 mean that the stenosis is severe, requiring surgical intervention, while FFR values above 0.8 mean the stenosis is mild and medication is sufficient. However, FFR values between 0.75 and 0.8 are intermediate stenoses, and medical doctors are unsure of the correct treatment for the patient. This non-dimensional parameter represents the ratio of the distal pressure (20mm downstream of the stenosis) and the aortic pressure. These pressure values are usually measured invasively in the coronary angiography medical procedure, where a pressure wire is inserted inside the blood vessel. This procedure captures the real value of the FFR, which essentially quantifies the pressure drop caused by the presence of the stenosis. However, the procedure has certain risks for the patients, especially ones with an advanced state of coronary artery disease.

As such, a non-invasive method of calculating the FFR is valuable to clinicians. There is a patented company named Heartflow® that already non-invasively measures the FFR. However, it is based in the USA, so medical doctors need to send patient data to this company. Moreover, the costs are around 1000 USD per patient, and it takes a few days to have the results.

The developed tool would be free, open source, and used on-site by medical doctors to obtain the FFR in a non-invasive way in less time (only a few hours). However, any tool used for medical purposes and applied in hospital settings must be thoroughly validated with many patient cases in order for the results to be trustworthy. The present tool has already been tested in one patient case with a mild stenosis (40% stenosis) and returned relative error value of 2.15% [2]. This is a promising result, but more patient cases should be tested.

The goal of this work is to validate the developed in-house computational tool that numerically predicts the FFR with a larger patient sample (four patients are analysed in the present work). The objective of the tool is to aid medical doctors in the diagnosis of coronary artery diseases, like atherosclerosis, and as a means to indicate the medical doctors the most appropriate treatment for each patient case. The tool uses complex models for blood and boundary conditions. A simplified Phan-Thien/Tanner (sPTT) model is used to represent the complex viscoelastic properties of blood and a three-element Windkessel model is used to model the pressure profile in four patient-specific coronary artery models. These have been obtained through the segmentation of Computed Tomography (CT) scans provided by the Centro Hospitalar de Vila Nova de Gaia e Espinho (CHVNG/E), whose medical doctors also measured patient-specific properties and the invasive value of the FFR. The comparison of the invasive FFR and the one obtained with the in-house computational tool using numerical methods is the basis for the validation of the latter. In this work, this comparison is performed for four patient cases, and the full validation will be done with many more patient cases. A statistical analysis was conducted to measure the performance of the model for four patient cases. The F1 score, accuracy, sensitivity, and specificity were assessed. These metrics provide insights into the ability of the model to non-invasively predict the FFR.

## 2 METHODOLOGY

The entire process used to determine the computed FFR is detailed in a previous paper [1], namely the creation of the patient-specific coronary artery, the replication of the artery in the hyperemia condition, the definition of the UDFs to define all boundary conditions, and the rheological model. The numerical settings used in the computational fluid dynamics (CFD) numerical simulations, conducted in ANSYS Fluent® 2023 software are also included in the

mentioned paper.

### 2.1 Patient data

Four patients were studied. Data regarding gender (female, F, or male, M), age, weight, height, body mass index (BMI) and body surface area (BSA) is presented in Table 1.

**Table 1**: Demographic and clinical data of patient cases.

| Patient case | Gender | Age | Weight [kg] | Height [cm] | BMI [$kgm^{-2}$] | BSA [$m^2$] |
|---|---|---|---|---|---|---|
| A | F | 58 | 73 | 155 | 30.4 | 17.7 |
| B | M | 61 | 94 | 155 | 39.1 | 20.1 |
| C | M | 66 | 79 | 175 | 25.8 | 19.6 |
| D | F | 70 | 58 | 162 | 22.1 | 16.2 |

These parameters were identified by medical doctors of CHVNG/E based on their described symptoms. CT scans of these patients revealed the presence of one or more stenosis inside the coronary artery tree. As seen in Figure 1, patient A exhibits a 90% stenosis within the LAD branch, patient B has a 60% stenosis detected in the LCX, patient C presents with a 60% stenosis in the LAD, and patient D has a significant 95% stenosis in the LAD.

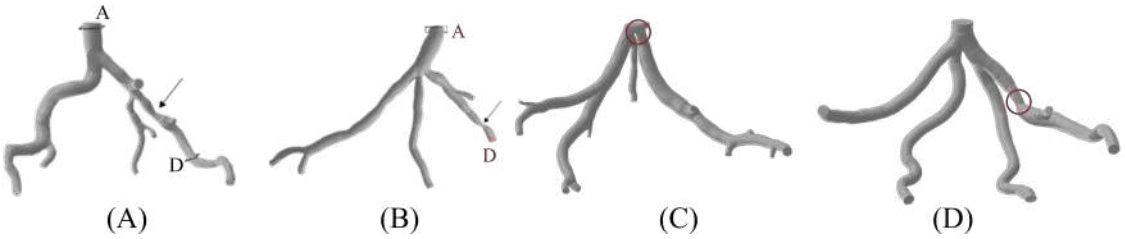


**Figure 1**: 3D models of the four patient cases (the stenoses are highlighted in red).

The invasive FFR values were measured for all the patient cases through catheterization, to be used to validate the numerical tool. In addition, the values of the systolic blood pressure (SBP), the diastolic blood pressure (DBP), and the heartbeat rate (HBR) were also measured, to be used in the modelling of the patient-specific boundary conditions. These properties are presented in Table 2.

It is known that hyperaemia conditions affect the geometry of the vessel, which impacts the flow properties. According to Wilson et al. (1990) [11], there is a 24bpm increase of the heartbeat rate, which leads to a decrease of the duration of the cardiac cycle. Therefore, the duration of the cardiac cycle of in hyperaemia conditions of patients A, B, C, and D can be calculated and it is equal to 0.7229s, 0.6522s, 0.7059s, 0.6522s, respectively.

### 2.2 3D model reconstruction and transformation into hyperaemia conditions

The geometries were constructed through image segmentation of the CT images provided by CHVNG/E, using the commercial software MIMICS®. Here, a semi-automatic method was

**Table 2**: Demographic and clinical data of patient cases in resting conditions.

| Patient case | Invasive FFR | SBP [mmHg] | DBP [mmHg] | HBR [bpm] |
|---|---|---|---|---|
| A | 0.58 | 135 | 67 | 59 |
| B | 0.89 | 134 | 76 | 68 |
| C | 0.81 | 155 | 101 | 61 |
| D | 0.61 | 151 | 88 | 68 |

used to reconstruct the lumen of the arteries case by case, through the selection of a point in the aorta, and the end point of all the branches. Then, the programmed automatically generated a model of the coronary artery which had a crass geometry due to the quality of the DICOM images and the segmentation methods used by the software.

Therefore, the 3D models had to be processed in 3-matic®, where the surfaces was smoothed and flat surfaces were created at the inlet and outlets (in order to create planes to apply the boundary conditions in ANSYS Fluent®).

Afterwards, the model was imported onto the commercial software Solidworks®, where the geometry was altered to account for the hyperaemia conditions: the cross-sectional area had to be increased 204% [11, 12]. As mentioned before, these are the conditions in which the FFR is measured invasively, so they must be replicated in a numerical environment.

More details regarding the 3D model reconstruction process and its transformation into hyperaemia conditions can be found in Fernandes et al. (2023) [1].

### 2.3 Mesh convergence test

For the numerical simulations, different mesh sizes were studied to find the one with the best balance between result accuracy and computational time. For all patients, uniform tetrahedron meshes were used with different number of elements, varying between 100000 and 700000.

After creating all the different meshes in ANSYS Meshing®, it was found they respected the standard skewness criteria [6, 1]. Therefore, another criterion needed to be added: running numerical simulations with the different mesh sizes, the aortic pressure was computed and, if its value varied a maximum of ±0.5% between consecutive meshes, then there was no more need to increase the number of elements.

The chosen meshes are displayed in Figure 2, and their properties can be found in Table 3. These were the meshes used in the numerical simulations.

**Table 3**: Mesh properties of the patients.

| Patient case | Minimum skewness | Maximum skewness | Average skewness | Standard deviation | Number of nodes | Number of elements |
|---|---|---|---|---|---|---|
| A | $1.5924\times10^{-3}$ | 0.6117 | 0.1325 | 0.1117 | 88742 | 489214 |
| B | $2.7843\times10^{-3}$ | 0.7262 | 0.1497 | 0.1216 | 40103 | 198563 |
| C | $7.522\times10^{-4}$ | 0.6567 | 0.1289 | 0.1092 | 128114 | 668665 |
| D | $2.9734\times10^{-3}$ | 0.6000 | 0.1310 | 0.1102 | 117994 | 611683 |

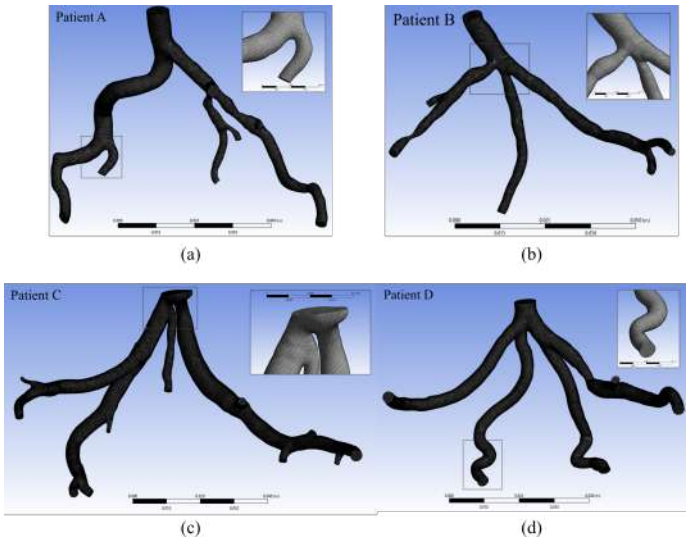


**Figure 2**: Mesh applied to patients: (a) A, (b) B, (c) C, (d) D.

### 2.4 Blood rheology, outlet pressure, and inlet velocity

In this section, the rheology model used to model blood as a viscoelastic fluid, called simplified Phan-Thien/Tanner (sPTT) model, is presented. Furthermore, the boundary conditions applied at the inlet and outlets of the coronary trees are described. In fact, a Womersley transient profile is applied at the inlet, and a three-element Windkessel model is used at the outlets. In both cases, patient-specific properties are incorporated in order to model the most real physiological conditions of the patient.

More details on blood rheology and the boundary conditions implemented as user-defined functions (UDFs) are described in detail in [2].

### 2.5 Simulation settings

For the measurement of the FFR, three planes were created:

**Table 4**: Properties of the defined planes used to numerically measure the FFR.

| Plane name | Generation | Location properties |
|---|---|---|
| Aortic | Automatic | Placed exactly 0.1 mm downstream the inlet surface<br>Parallel to the inlet |
| Stenotic | Manual | Centre of the stenosis<br>Normal to the centreline |
| Distal | Automatic | Placed exactly 20 mm downstream the stenotic plane<br>Normal to the centreline |

The location of the aortic and distal planes in the 3D models can be seen in Figure 3. For patient B, the distal plane could not be created because its location stood outside of the 3D model. The closest outlet surface was chosen instead.

Running the numerical simulations, the area-average total pressure values on the aortic and

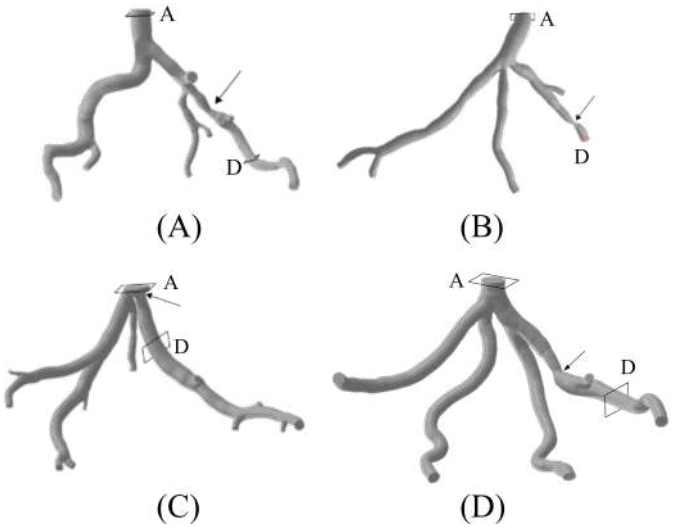


**Figure 3**: Location of the aortic [A] and distal [D] planes in the 3D models of the coronary arteries (stenoses signaled with an arrow).

distal planes were retrieved. Applying the trapezoidal rule, representative pressure values of the entire cardiac cycle were calculated and used to determine the numerical FFR:

$$p = \frac{1}{T}\int_0^T p_d \, dt \approx \frac{\Delta t}{2T}\left(p_0 + 2p_1 + 2p_2 + ... + 2p_{n-1} + p_n\right) \tag{1}$$

In equation 1, $\Delta t$ is the time step size (defined as 0.005s for all numerical simulations), $T$ is the duration of the cardiac cycle, and $n$ is the total number of time steps (equal to the division of $T$ by $\Delta t$). As mentioned before, $T$ of in hyperaemia conditions of patients A, B, C, and D is 0.7229s, 0.6522s, 0.7059s, 0.6522s, respectively. Therefore, $n$ is 145, 131, 142, and 131 per cardiac cycle of patients A, B, C, and D, respectively.

Five cardiac cycles were ran for all patients to reduce initialization errors, and only the data computed during the fifth cycle was used to calculate the numerical FFR.

## 3 RESULTS

In this section, the results of the numerical FFR and the relative error between the invasive and the numerical FFR are presented, as well as a statistical analysis.

### 3.1 FFR results

A comparison between the invasive FFR values obtained by medical doctors and the numerical values obtained through the in-house computational tool using numerical simulations can be found in Table 5.

The relative error was very high for patient B. As seen in Figure 1, the real distal plane is not present in the 3D model, so the distal plane could not be created. Therefore, the distal pressure captured is not the same measured invasively. The flow recuperates after the obstacle (the stenosis), and this did not occur at the recorded distal plane.

**Table 5**: Invasive and computed FFR values for each patient case.

| Patient case | Invasive FFR | Numerical FFR | Relative error [%] |
|---|---|---|---|
| A | 0.58 | 0.497 | 14.3 |
| B | 0.89 | 0.156 | 82.5 |
| C | 0.81 | 0.904 | 11.6 |
| D | 0.61 | 0.535 | 12.3 |

Regarding patient C, there is also uncertainty in the distal pressure results. Initially, the numerical FFR was 0.618, which returned a relative error in comparison with the invasive FFR of 23.7%. This happens because it was found that the distal plane encompassed cross-sections of other artery branches (Figure 4). Therefore, the automatic creation of the aortic and distal planes needs to be verified by the user before running the numerical simulations. As a solution, Fluent® has a tool to manually clip planes to only consider the points that fall within a specific range of x, y, and/or z coordinates. It was found that in the desired plane (in green in Figure 4), the values of y are between -0.005 m and 0.0045 m. Considering only those specific coordinates, the FFR was recalculated and, as seen in Table 5, the updated value is 0.904, which corresponds to a relative error of 11.6%. These are the correct values.

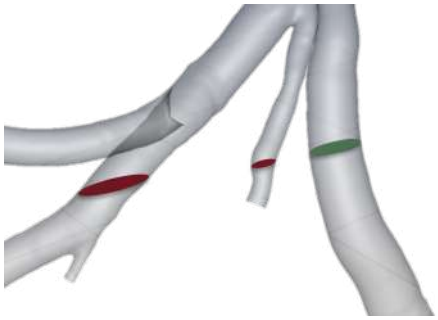

**Figure 4**: Distal plane of patient C.

### 3.2 Statistical analysis of the results

The correlation between the invasive and numerical FFR of patients A, C, and D, as well as the initial patient studied in previous works (Fernandes et al. (2023) [1]) is displayed in Figure 5. This patient has a 40% stenosis in the proximal area of the left anterior descending artery, and possessed an invasive FFR of 0.93. The patient is a 63-year-old male, with a resting HBR of 59bpm, SBP and DBP equal to 125.3mmHg and 84.6mmHg, respectively. After performing numerical simulations, a numerical FFR of 0.905 was obtained, which corresponds to an error of 2.15%. This extra patient is also considered in the data used for the statistical analysis performed in this Subsection, named patient E.

The overlap between the values is very high, which means there is a good agreement between the invasive and numerical FFR values. However, the current results seem to indicate that the tool should not be used as a regression tool, i.e. to determine the exact value of the FFR, but

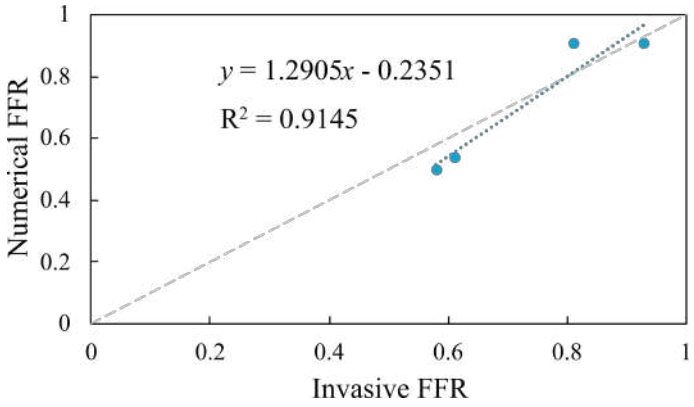


**Figure 5**: Correlation between invasive and numerical FFR values of several patients.

instead as a classification tool, i.e. to determine the range of the stenosis as mild, intermediate, or severe. In fact, the average relative error between the invasive and numerical FFR is 10.2%, the median is 11.6% and the standard deviation is 5.1%.

The tool can be a binary classification one, with two possible answers: the tool is accurate in defining the type of stenosis or it is not. To statistically assess our numerical tool as a classification tool, two threshold values (TVs) for defining positive and negative cases were considered, equal to 0.75 and 0.8 (which are the limits of the mild, intermediate and severe stenoses).

There are four possible outcomes: a true positive (TP), where both the invasive and numerical FFR values are below TV, a true negative (TN), where both the invasive and numerical FFR values are higher or equal to TV, a false positive (FP), where the invasive FFR is higher or equal to TV but the numerical FFR is lower than TV, and, finally, a false negative (FN), where the invasive FFR is lower than TV but the numerical FFR is higher or equal to TV [15].

### 3.2.1 Accuracy, sensitivity, and specificity

The accuracy is the ratio of correct assessments of both true positives and true negatives to the number of all assessments, and it is a measure of the overall correctness of our prediction model. The sensitivity is a measure of the proportion of actual positives that are correctly identified by the tool, and it is calculated as the ratio of true positive assessments to the number of all positive assessments. The specificity measures the proportion of actual negatives that are correctly identified, and it is the ratio of true negative assessments to the number of all negative assessments [15].

From the results, regardless of the TV, it is possible to conclude that patients A and D are true negatives and patients C and E are true positives, and there are no false positives or false negatives [15]. The previous three parameters can be calculated as:

$$\text{Accuracy} = \frac{TP + TN}{TP + TN + FP + FN} \tag{2}$$

$$\text{Sensitivity} = \frac{TP}{TP + FN} \tag{3}$$

$$\text{Specificity} = \frac{TN}{TN + FP} \tag{4}$$

### 3.2.2 Precision and F1 score

For binary classification systems, the F1 score can also be used to assess the accuracy of the numerical tool. It is computed through the precision (the total number of real positive results by the total number of samples that were expected to be positive) and recall (the same expression for the sensitivity). It is calculated as:

$$\text{Precision} = \frac{TP}{TP + FP} \tag{5}$$

$$\text{Recall} = \text{Sensitivity} \tag{6}$$

$$\text{F1 Score} = 2 \times \frac{\text{Precision} \times \text{Sensitivity}}{\text{Precision} + \text{Sensitivity}} \tag{7}$$

$$\tag{8}$$

The results are summarized in Table 6.

**Table 6**: Statistical metrics used to evaluate the performance of the in-house FFR calculation tool for a threshold value of 0.75 and 0.80.

| Statistical metric | Value for TV = 0.75 | Value for TV = 0.8 |
|---|---|---|
| Accuracy | 1 | 1 |
| Sensitivity | 1 | 1 |
| Specificity | 1 | 1 |
| F1 score | 1 | 1 |

## 4 CONCLUSIONS

Several conclusions can be outlined from the developed work.

The FFR values obtained through out software were, as indicated by the results of the statistical analysis, similar to the invasive results. In fact, the average relative error between the two FFR values is 10.2%, the median is 11.6% and the standard deviation is equal to 5.1%. Overall, the developed in-house software was able to correctly categorize the mild (FFR $> 0.8$) and severe (FFR $< 0.75$) stenoses.

Therefore, the statistical analysis shows that the numerical tool can be used for the classification of the FFR in different ranges (above or below 0.8 or 0.75). Our results indicate that this computational tool has returned information similar to the medical procedures carried out in the hospital. It is known that these procedures are costly for the hospital and are time-consuming and, with proper validation, this tool could aid the diagnostic procedure in-situ and without costs.

Therefore, the collaboration between medical doctors and researchers is essential for developing advanced tools that have the potential to aid the diagnostic and indicate the proper treatment on a case-by-case basis, which could improve patient care. In the future, it could be possible that the FFR is fully measured non-invasively, turning the currently invasive practices into obsoletes practices.

## 5 STUDY LIMITATIONS AND FUTURE WORK

Even though this study has shown promising results, the current state of this tool has some limitations.

The invasive measurement of the FFR may not be fully accurate for a few reasons, like the movement of the patient during the measuring procedure, or diminishing effects of the hyperaemia induction (waiting too long after its administration to perform the pressure measurements). Therefore, in addition to the invasive FFR measured at the hospital, other forms of validation should be used, like in-vitro experimental trials or data from the patented company Heartflow®.

Moreover, before the implementation of this tool in hospitals is possible, many more patients need to be tested to ensure accuracy and representability of as many patients as possible, specially in regards to the degree of severity of the stenoses. In particular, our tool should be tested in intermediate stenosis ($0.75 < \text{FFR} < 0.80$).

All in all, the aim of this work is to obtain a validated numerical tool that returns a numerical FFR that differs from the invasive value by less than 5%. To achieve this, there will be 2 types of validation: the invasive FFR and the value measured by the patented company Heartflow®. This process will, in the future, allow a thorough validation of the results of the developed software.

## ACKNOWLEDGEMENTS

Authors gratefully acknowledge the financial support of FCT, the Foundation for Science and Technology (Portugal), regarding the R&D Project "CADS-FACT-PTDC / EMD-EMD / 0980 / 2020", the Engineering Faculty of University of Porto (FEUP), the Institute of Science and Innovation in Mechanical and Industrial Engineering, (LAETA-INEGI), the Cardiovascular R&D Unit of the Medicine Faculty of University of Porto (FMUP), and the Cardiology Department of Gaia/Espinho Hospital Centre (CHVNG/E).

## REFERENCES

[1] M. Fernandes, L.C. Sousa, C.A.C. António, and S.I.S. Pinto. 2023. "Modeling the Five-Element Windkessel Model with Simultaneous Utilization of Blood Viscoelastic Properties for FFR Achievement: A Proof-of-Concept Study." Mathematics 11, no. 24: 1-19. https://doi.org/10.3390/math11244877.

[2] M. Fernandes, L.C. Sousa, C.C. António, and S.I.S. Pinto. 2024. "Accuracy and temporal analysis of non-Newtonian models of blood in the computational FFR – Numerical implementation." International Journal of Non-Linear Mechanics 161: no. May: 1-9. https://doi.org/10.1016/j.ijnonlinmec.2024.104683.

[3] A. Dash, K. Jain, N. Ghosh, and A. Patra. 2022. "Non-invasive detection of coronary artery disease from photoplethysmograph using lumped parameter modelling." Biomedical Signal Processing and Control 77: no. April: 1-11. https://doi.org/10.1016/j.bspc.2022.103781.

[4] P. Meimoun, J. Clerc, D. Ardourel, U. Djou, S. Martis, T. Botoro, F. Elmkies, H. Zemir, A. Luycx-Bore, and J. Boulanger. 2017. "Assessment of left anterior descending artery stenosis

of intermediate severity by fractional flow reserve, instantaneous wave-free ratio, and non-invasive coronary flow reserve." International Journal of Cardiovascular Imaging 33, no. 7: 999-1007. https://doi.org/10.1007/s10554-016-1000-3.

[5] X. Liu, C. Xu, S. Rao, Y. Zhang, D. Ghista, Z. Gao, and G. Yang. 2022. "Physiologically personalized coronary blood flow model to improve the estimation of noninvasive fractional flow reserve." Med. Phys 49, no. 2022: 583-597. https://doi.org/10.1002/mp.15363.

[6] P. Kohnk. 2009. "Ansys Theory Reference for the Mechanical APDL and Mechanical Applications." 3304: 724-746.

[7] L. Campo-Deano, R. Dullens, D. Aarts, F. Pinho, and M. Oliveira. 2013. "Viscoelasticity of blood and viscoelastic blood analogues for use in polydymethylsiloxane in vitro models of the circulatory system." Biomicrofluidics 7, no. 3: 1-12. https://doi.org/10.1063/1.4804649.

[8] A. Jonasova, and J. Vimmr. 2021. "On the relevance of boundary conditions and viscosity models in blood flow simulations in patient-specific aorto- coronary bypass models." International Journal for Numerical Methods in Biomedical Engineering 37, no. 4: 1-14. https://doi.org/10.1002/cnm.3439.

[9] S. Kwon, E. Chung, J. Park, G. Kim, J. Kim, K. Kim, E. Shin, and E. Shim. 2014. "A novel patient-specific model to compute coronary fractional flow reserve." Progress in Biophysics and Molecular Biology 116 no. 1: 48-55. https://doi.org/10.1016/j.pbiomolbio.2014.09.003.

[10] T. Duguay, C. Tesche, R. Vliegenthart, C. De Cecco, H. Lin, M. Albrecht, A. Varga-Szemes, D. De Santis, U. Ebersberger R. Bayer, S. Litwin, E. Hoffmann, D. Steinberg, and U. Schoepf. 2017. "Coronary Computed Tomographic Angiography-Derived Fractional Flow Reserve Based on Machine Learning for Risk Stratification of Non-Culprit Coronary Narrowings in Patients with Acute Coronary Syndrome." American Journal of Cardiology 120, no. 8: 1260-1266. https://doi.org/10.1016/j.amjcard.2017.07.008.

[11] R.F. Wilson, K. Wyche, B.V. Christensen, S. Zimmer, and D.D. Laxson. 1990. "Effects of adenosine on human coronary arterial circulation." Circulation 82, no. 5: 1595-1606. https://doi.org/10.1161/01.CIR.84.5.2208.

[12] P. Sharma, L. Itu, X. Zheng, A. Kamen, D. Bernhardt, C. Suciu, and D. Comaniciu. 2012. "A Framework for Personalization of Coronary Flow Computations During Rest and Hyperemia." In 34th Annual International Conference of the IEEE EMBS: 6665-6668. https://doi.org/10.1109/EMBC.2012.6347523.

[13] A. Coenen, A. Rossi, M. Lubbers, A. Kurata, A. Kono, R. Chelu, S. Segreto, M. Dijkshoorn, A. Wragg, R. van Geuns, F. Pugliese, K. Nieman. 2017. "Integrating CT Myocardial Perfusion and CT-FFR in the Work-Up of Coronary Artery Disease." JACC: Cardiovascular Imaging 10 no. 7: 760-770. https://doi.org/10.1016/j.jcmg.2016.09.028.

[14] R. Nakazato, H. Park, D. Berman, H. Gransar, B. Koo, A. Erglis, F. Lin, A. Dunning, M. Budoff, J. Malpeso, J. Leipsic, J. Min. 2013. "Noninvasive fractional flow reserve derived from computed tomography angiography for coronary lesions of intermediate stenosis severity results from the DeFACTO study." Circulation: Cardiovascular Imaging 6 no. 6: 881-889. https://doi.org/10.1161/CIRCIMAGING.113.000297.

[15] W. Zhu, N. Zeng, N. Wang. 2010. "Sensitivity, specificity, accuracy, associated confidence interval and ROC analysis with practical SAS® implementations." Conference Proceedings: Northeast SAS Users Group 2010: 1-9. https://www.lexjansen.com/cgi-bin/xsl_transform.php?x=NESUG2010.